Journal of Alloys and Compounds 496 (2010) 500–507

Contents lists available at ScienceDirect

Journal of Alloys and Compounds

journal homepage: www.elsevier.com/locate/jallcom

Influence of chloride, sulfate and bicarbonate anions on the corrosion behavior of AZ31 magnesium alloy

Lei Wang[a,b], Tadashi Shinohara[b,*], Bo-Ping Zhang[a]

[a] School of Materials Science and Engineering, University of Science and Technology Beijing, Beijing 100083, China
[b] Materials Reliability Center, National Institute for Materials Science, 1-2-1 Sengen, Tsukuba 305-0047, Japan

ARTICLE INFO

Article history:
Received 9 October 2009
Received in revised form 8 February 2010
Accepted 11 February 2010
Available online 18 February 2010

Keywords:
Magnesium
AZ31 alloy
Electrochemical measurements
Dilute solutions
Corrosion maps

ABSTRACT

Influence of chloride, sulfate and bicarbonate anions on the corrosion behavior of AZ31 magnesium alloys in dilute solutions was investigated by electrochemical measurements, whereby corrosion maps in terms of electrode potential and solution concentration were obtained. AZ31 alloy exhibited corrosion and passivation zones in those dilute solutions. The passivation zone was strongly influenced by the kinds of the solution used and the broadest zone was obtained in Na_2SO_4, followed by NaCl and $NaHCO_3$. AZ31 alloy had a better corrosion resistance in Na_2SO_4, attributing to the lowest attack by SO_4^{2-} and a thick corrosion product covering the surface which inhibited the corrosion attack. However, despite a much lower passivation zone in $NaHCO_3$ as compared to the other two solutions, the corrosion rate in $NaHCO_3$ was found to be the lowest. The values of open-circuit potential were in the passivation zone when [Cl^-] was less than 0.2 mol/L in NaCl, and [SO_4^{2-}] and [HCO_3^-] were both less than 0.3 mol/L in Na_2SO_4 and $NaHCO_3$. In the passivation zone, the formation of surface films or corrosion products on the material surface retarded further corrosion in dilute solutions. In the corrosion zone, pits grew continuously in depth and diameter in NaCl and Na_2SO_4 resulting in the localized corrosion through the agglomeration of pits. The formation of crystalline-like $MgCO_3$ products exhibited the general corrosion in $NaHCO_3$.

1. Introduction

Magnesium and its alloys are widely used as structural materials because of their unique physical and mechanical properties such as low density and high strength-to-weight ratio. One of the important applications of these alloys is for the automotive industry, where the reduction of the total weight of a vehicle leads to fuel efficiency and pollution reduction. Being the most electrochemically active metal used for structural purposes, magnesium and its alloys were characterized as having relatively poor corrosion resistance, especially in marine environments [1–5].

Magnesium alloys usually suffer from rapid corrosion in the presence of sodium chloride in humid air. Their surfaces often are covered white, flaky corrosion products of magnesium hydroxide in such environments [6–9]. However, Shinohara and Wang [10] reported that the corrosion behavior of AZ31 magnesium alloy is insensitive to the atmospheric exposure environment. Their report implied that the test coupons reveal a good resistance during raining and it is important to understand the corrosion behavior of magnesium alloy in dilute solutions.

Most studies in the literature of magnesium alloys focused on the role of Cl^- in the corrosion process, and in particular the anodic dissolution mechanism [6–9,11–15]. Few studies in the literature has been concerned the corrosion behavior of magnesium alloys in aqueous solutions of SO_4^{2-} and HCO_3^-. Many aspects of the corrosion performance of magnesium alloys in dilute solutions of both ions are of great importance and still remain ill-defined. The effect of carbon dioxide and sulphur dioxide is also important, especially in the atmospheric environment. The corrosion behavior of AZ31 magnesium alloy in dilute NaCl solutions was studied previously and there are the corrosion and passivation zones for this material in dilute solutions [16]. This paper extended the detailed study to the changes of corrosion behavior of AZ31 alloy in Na_2SO_4 and $NaHCO_3$ using electrochemical measurements as comparing to NaCl.

2. Experimental

Experiments were performed on a commercially extruded AZ31 magnesium alloy with the chemical composition shown in Table 1. The tested specimens were cylindrical in shape with the dimension of 10 mm × 10 mm. The specimens were connected to lead wires and embedded in epoxy resins except the exposed surfaces. The exposed surfaces were mechanically polished up to 1200 grit SiC paper, then polished with a silica slurry, and finally rinsed with ethanol.

The test specimens were subjected to nondeaerated aqueous solutions of 0.01–0.3 mol/L NaCl [16], Na_2SO_4 and $NaHCO_3$ at room temperature. In the nondeaerated condition, the specimens were tested in the solutions open to air. The

* Corresponding author. Tel.: +81 29 859 2604; fax: +81 29 859 2601.
E-mail address: SHINOHARA.Tadashi@nims.go.jp (T. Shinohara).

0925-8388/$ – see front matter © 2010 Elsevier B.V. All rights reserved.
doi:10.1016/j.jallcom.2010.02.088

Table 1
Chemical composition of AZ31 alloy (wt.%).

	Al	Zn	Mn	Si	Cu	Ni	Fe	Mg
AZ31	3.05	0.82	0.40	0.020	0.003	0.0012	0.0023	Bal.

open-circuit potential (E_{ocp}) values of the specimens were monitored in the solutions for 72 ks using an SDPS-501C electrochemical analyzer (SYRINX Inc., Japan). Cathodic and anodic potentiodynamic polarization tests were performed at a scan rate of 0.17 mV/s using the SDPS-501C electrochemical analyzer. A saturated calomel electrode (SCE) and a 0.125 mm thick platinum foil (10 mm × 20 mm) were used as the reference electrode and the counter electrode, respectively. The starting potentials of the cathodic polarization were −1.70 V in NaCl and Na_2SO_4 and −2.30 V in $NaHCO_3$, respectively. The corrosion potential (E_{corr}, given by the machine) was the starting point for anodic polarization. Potentiostatic polarization tests were performed to observe the initiation and growth of pits using an SDPS-308 electrochemical analyzer (SYRINX Inc., Japan), in which the specimens were polarized immediately at a given potential after immersion and maintained at this potential for a given duration (3.6 ks, 18 ks, 36 ks, and 72 ks). For all the measurements, the same test was repeated at least twice.

The polarized surface morphology was characterized using a laser microscope (LM, VK-8500, KEYENCE Inc., Japan). The corrosion products on the surface were removed using a reagent of 5 g Cr_2O_3 and 0.25 g $AgNO_3$ in 25 mL deionized water. The maximum corrosion depth was determined based on the depth profile measured by LM.

3. Results and discussion

3.1. Electrochemical measurements

Fig. 1 shows the time variations of the E_{ocp} for AZ31 in 0.01–0.3 mol/L NaCl [16], Na_2SO_4 and $NaHCO_3$ solutions for 72 ks. The specimens exhibit a definite decrease in E_{ocp} values with increasing [Cl^-] and [HCO_3^-] (Fig. 1(a) and (c)), whereas the specimen exhibits a slight change in E_{ocp} in Na_2SO_4 (Fig. 1(b)). This indicates that the growth of surface films or corrosion products probably does not strongly depend on the SO_4^{2-} concentration. The E_{ocp} value initially enhances quickly and then increases slowly in the lower concentrated 0.01 mol/L NaCl, which is attributed to the stable growth of the protective surface film formed with Mg^{2+} and OH^- ions. The E_{ocp} shift to more noble values, albeit with frequent fluctuations, after showing a rise and a drop in 0.03–0.3 mol/L NaCl. This indicates that the surface films were firstly attacked by Cl^- ion and then passivated with the corrosion products with increasing immersion time [16]. The fluctuation of E_{ocp} is probably due to the fluctuation of the pH near the surface [17,18]. Those specimens exposed to Na_2SO_4 and $NaHCO_3$ solutions exhibit the initial increase rapidly and then rise slowly in E_{ocp}. In $NaHCO_3$, this increasing trend means that the surface film formed with Mg^{2+} and CO_3^{2-} ions likely plays a protective role with time.

Fig. 2 shows the cathodic and anodic polarization curves of AZ31 in 0.01–0.3 mol/L NaCl [16], Na_2SO_4 and $NaHCO_3$ solutions. All specimens show similar cathodic polarization behavior, in which the cathodic current densities rise rapidly from E_{corr} and then increase slowly to −1.70 V (in NaCl and Na_2SO_4) and −2.30 V (in $NaHCO_3$). They exhibit no appreciation of this type of behavior with increasing solution concentrations. On the other hand, the anodic current densities depend on the solution concentrations for all of the specimens. Song et al. [19] considered that the cathodic process might only make the surface film thinner with the hydrogen evolution occurred mainly on the surface film in NaCl solutions. However, in their case, magnesium dissolution into solution at an applied anodic potential occurred mainly at the broken area of the film. This means that the increasing Cl^- concentration caused an enhance in the current density and provided a larger area for anodic dissolution, which is assumed that the anodic process was much more sensitive to Cl^- concentration than the cathodic process. In our study, it could be considered that the anodic process was much more sensitive than the cathodic process to Cl^-, SO_4^{2-} and HCO_3^- concentrations.

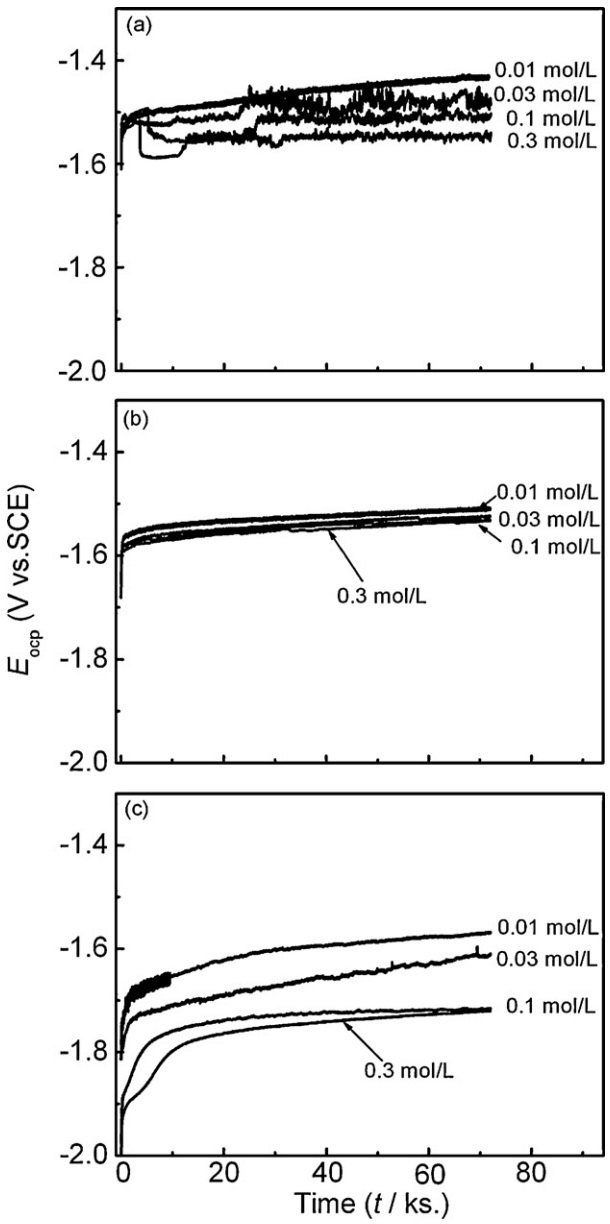

Fig. 1. Time variations of open-circuit potentials on AZ31 alloy in various concentrations of (a) NaCl [16], (b) Na_2SO_4 and (c) $NaHCO_3$ solutions.

The E_{corr} values shift in the negative direction with increasing [Cl^-] and [HCO_3^-] (Fig. 2(a) and (c)), which agree with the decreased E_{ocp} with increasing [Cl^-] and [HCO_3^-] (Fig. 1(a) and (c)). Following Brillas et al. [20], the potential shifted in the negative direction was related with a greater activity of the alloy, it is possible that magnesium chloride or carbonate produced film defects which enable an easier ingress of aggressive Cl^- and HCO_3^- anions. The E_{corr} in Na_2SO_4 (Fig. 2(b)) exhibits a similar value which is consistent with the E_{ocp} (Fig. 1(b)). On the other hand, the curves show an apparent Tafel region in NaCl and Na_2SO_4, whereas those in $NaHCO_3$ increase quickly and then exhibit almost constant values probably attributing to a protective layer formed with HCO_3^-. The specimens in NaCl exhibit a passivation and their passive current densities, i, are less than 100 μA/cm^2. The potential at which the i is 100 μA/cm^2 was defined as a pitting potential [16] since the i increases quickly up to 100 μA/cm^2. In Na_2SO_4, a current plateau

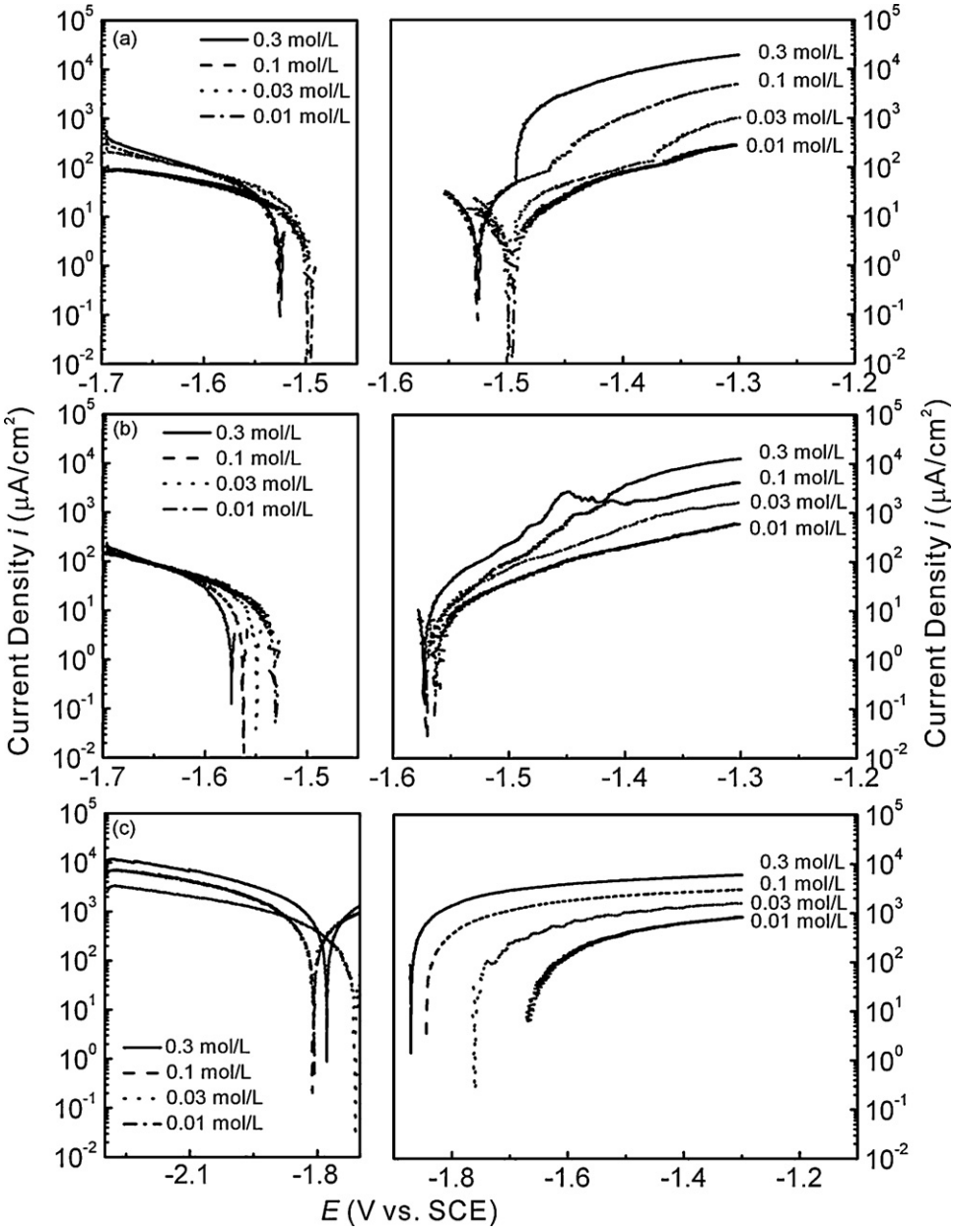

Fig. 2. Cathodic and anodic polarization curves for AZ31 alloy in various concentrations of (a) NaCl [16], (b) Na_2SO_4 and (c) $NaHCO_3$ solutions.

is observed and its height depends on the SO_4^{2-} concentration. Pits were also observed on the surface when the i rises to 100 μA/cm^2, although the specimens do not show an obvious passive region in the anodic polarization curves.

Fig. 3 shows the typical time variations of the current densities on AZ31 polarized potentiostatically in 0.01 mol/L NaCl [16], Na_2SO_4 and $NaHCO_3$ solutions at various potentials within the range of −1.50 to −1.30 V. In NaCl (Fig. 3(a)), the specimen polarized at −1.50 V shows the passivation state in stage II, and that at −1.44 V after 10.8 ks polarization also comes into the passivation state after showing the corrosion. This later behavior suggests that the corrosion product precipitates inside the pits and retards their pits growth, leading to the hindrance of current density flowing through the pits. The specimens polarized at −1.40 V and −1.35 V show the corrosion state in stage III as the i increases up to above 100 μA/cm^2. In Na_2SO_4 (Fig. 3(b)), when the potentials were at −1.50 V, −1.45 V, and −1.40 V, the i values increase abruptly to peak values 50–150 μA/cm^2 and then decrease to reach constant values at 0–10 μA/cm^2 until polarization of 72 ks showing the passivation. In the case at −1.35 V, the i increases rapidly to 500 μA/cm^2 and decreases to 200 μA/cm^2 after 3.6 ks polarization and then increases again to a steady value of around 250 μA/cm^2 indicating the corrosion. In the passivation state, pit growth is therefore arrested and metal dissolution is controlled by the rate of ionic migration through the salt film or corrosion products formed over the active surface of pits. In $NaHCO_3$ (Fig. 3(c)), all specimens show a similar tendency in the current density, in which the i values show a maximum at the early stage of polarization at −1.50 to −1.30 V, followed by a decay reaching to a relatively low values after the formation of the anodic film or product [21,22]. The initial increasing trend may be attributed to a reduced surface electrolyte pH which acts to enhance the dissolution rate of the surface film. The specimen polarized at −1.50 V shows the passivation state in stage II as the i is 20 μA/cm^2 around after 72 polarization, while the specimens polarized at −1.45 to −1.30 V show the corrosion state.

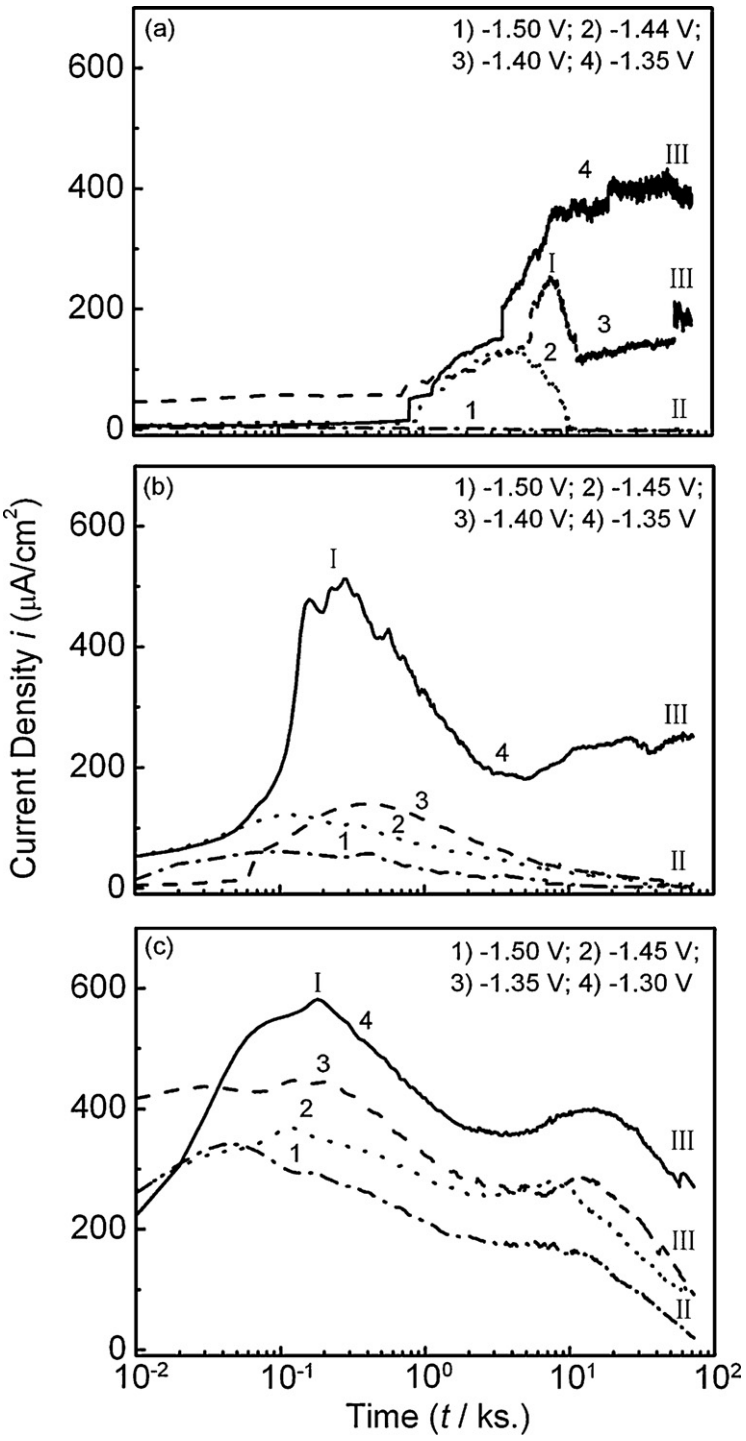

Fig. 3. Time variations of current densities on AZ31 alloy polarized potentiostatically in 0.01 mol/L (a) NaCl [16], (b) Na_2SO_4 and (c) $NaHCO_3$ solutions for 72 ks at various potentials. (I, II, and III represent activation, passivation and corrosion states, respectively.)

Compared to NaCl, the *i* values rapidly ascend to a maximum in Na_2SO_4 and $NaHCO_3$ from the moment just after immersion. This indicates the breakdown of the surface layers initially induced by attack from SO_4^{2-} and HCO_3^- ions. Meanwhile, these layers in Na_2SO_4 and $NaHCO_3$ have a poor barrier effect compared to the layer in NaCl in the early period of polarization. After the peak *i*, the fall of current transient suggests the thickening of the surface film or the corrosion product until polarization to 72 ks [21,23,24]. This behavior also means that the barrier effect of the surface layer on the material in Na_2SO_4 and $NaHCO_3$ is higher than that in NaCl after 3.6 ks polarization.

3.2. Corrosion morphology and corrosion depth

Fig. 4 shows the micrographs of AZ31 polarized potentiostatically in 0.01 mol/L NaCl, Na_2SO_4 and $NaHCO_3$ solutions at various potentials for 72 ks. In all solutions, hydrogen gas bubbles were observed just after polarization started. In the case of NaCl, a passivation film is observed on the surface of the specimen polarized at −1.50 V. Pitting and filiform corrosion are evident in the polarization range of −1.44 to −1.35 V that the thickness and the amount of the corrosion layer enhances with increasing polarization potentials. In the case of Na_2SO_4, the thick passivation films occur on

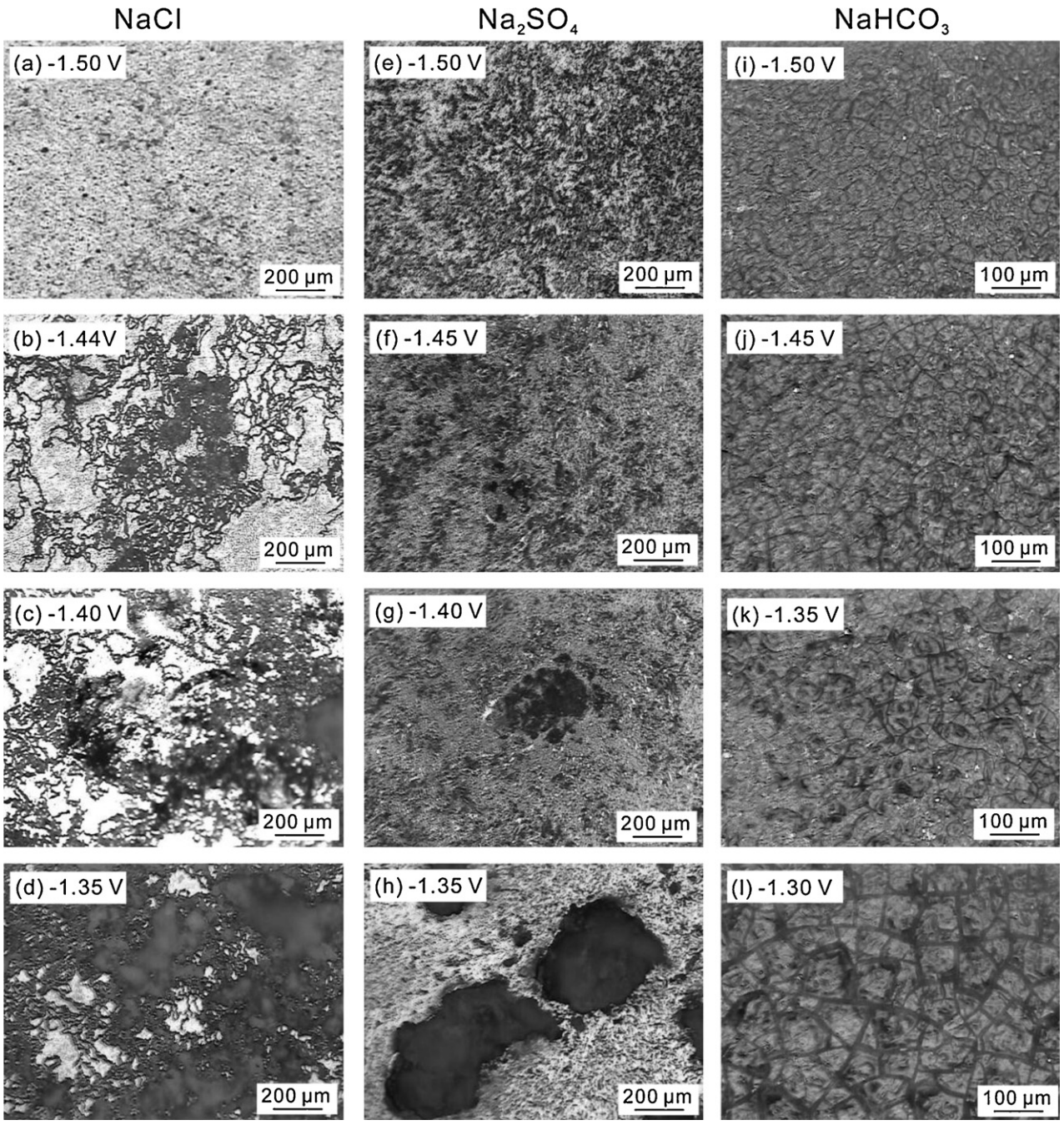

Fig. 4. Morphologies of AZ31 alloy polarized potentiostatically in 0.01 mol/L (a–d) NaCl, (e–h) Na_2SO_4 and (i–l) $NaHCO_3$ solutions for 72 ks at various potentials.

the surfaces polarized at −1.50 to −1.40 V, and shallow pits are observed at −1.40 V due to the release of hydrogen bubbles. At −1.35 V of polarization, pits ranging 400–600 μm in diameter are found on the material. From the results described above, it can be concluded that the specimen polarized at −1.40 V in NaCl suffers localized corrosion, while that at the same potential in Na_2SO_4 stays in the passive state.

Since potentiodynamic polarization (Fig. 2(a)) shows a defined E_{pit} (V'_{c100}) in the early stage, the corrosion process should be associated with pitting attack in the potentiostatic polarization. Pitting corrosion of magnesium alloys is due to the adsorption followed by localized penetration of aggressive anions (Cl^- and SO_4^{2-} in this study) under polarized potential through the passive film at the micro-structural defect sites [25]. The more positive is the polarized potential, the more will be the active sites available for pit nucleation. In addition, an increase in the polarized potential may increase the electric field across the passive film and therefore enhance the adsorption of Cl^- and SO_4^{2-} anions. The adsorbed Cl^- and SO_4^{2-} anions tend to enhance the dissolution of surface film. In previous study [26], an increased adsorption of Cl^- was found in corroded area using XPS method. In this study, the pits grow and connect resulting in the localized corrosion distributed by the filiform and pitting products with polarization time. The filiform mode of corrosion may be due to a switch from oxygen reduction on the surface to hydrogen evolution at weak areas in the initial film [27].

On the other hand, a different type of corrosion attack appears on the surfaces polarized at −1.50 to −1.30 V in $NaHCO_3$, This attack is characterized by the formation of a crystalline-like film or product showing the general corrosion. A crackled appearance presented

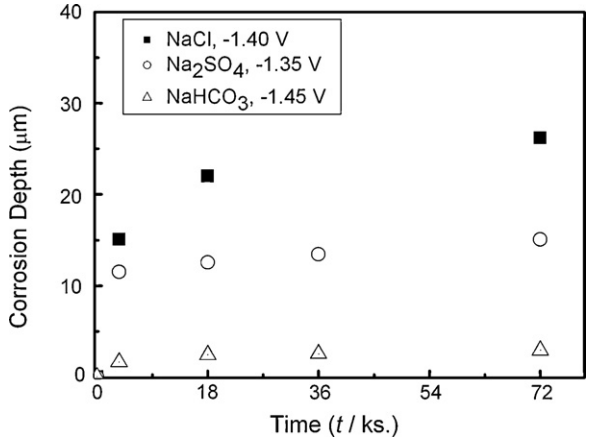

Fig. 5. Time variations of corrosion depths on AZ31 alloy polarized potentiostatically in 0.01 mol/L NaCl, Na_2SO_4 and $NaHCO_3$ solutions at various potentials.

on all the surfaces may have been caused by the dehydration of the layers after drying in air. Lindström et al. [27] thought that the characteristic filiform attack was connected to the initial air-formed film in the atmospheric exposure containing 350 ppm CO_2. After a longer exposure, the filiform attack was replaced by the development of numerous, microscopic electrochemical cell that created a thick, carbonate-containing film covering the whole surface. In this work, the protolysis of HCO_3^- counteracts the development of pH gradients on the surface after a long polarization, impeding the development of corrosion cell and resulting in the inhibition of pitting corrosion. Further, it obviously shows that the pitting corrosion is much pronounced in the solutions containing Cl^- and SO_4^{2-}.

Fig. 5 shows the time variations of the maximum corrosion depths for AZ31 polarized potentiostatically in 0.01 mol/L NaCl, Na_2SO_4 and $NaHCO_3$ solutions. We chose the potentials in stage III (Fig. 3), in which the maximum pit depths in NaCl and Na_2SO_4 and corrosion depth in $NaHCO_3$ were detected, respectively. All specimens show a rapid rise within 3.6 ks polarization and then a slow increase to 72 ks polarization. This behavior is attributed to the ions attacking the surface leading to anodic dissolution of the material. The pit depth in Na_2SO_4 at −1.35 V rises from 11 μm to 15 μm within the range of 3.6–72 ks polarization, while that in NaCl at −1.40 V increases from 15 μm to 26 μm. The latter presents the most significant change as compared to Na_2SO_4 and $NaHCO_3$. Even though the current density is high (Fig. 3(c)), the specimen in $NaHCO_3$ exhibits the shallowest corrosion depth (about 2 μm) due to general corrosion. Due to the relatively higher i (>20 μA/cm^2) in the potentiostatic experiments and the continuous increase in the corrosion depth for AZ31 alloy, these potentials are considered as the critical pitting potentials (V_c) for the propagation of pits in 0.01 mol/L NaCl and Na_2SO_4 and the corrosion potential in 0.01 mol/L $NaHCO_3$, respectively. Using the same method, V_c in 0.03–0.3 mol/L solutions were also measured for all the specimens.

3.3. Corrosion map

Fig. 6 shows the corrosion maps for AZ31 obtained in terms of electrode potential and [Cl^-], [SO_4^{2-}] and [HCO_3^-] according to electrochemical measurements. All specimens exhibit corrosion and passivation zones in various solutions (the immunity for magnesium occurs in the potentials lower than −2.6 V (vs. SHE) [28]). The E^0_{ocp} were determined as E_{ocp} values after 72 ks polarization in solutions. V'_{c100} were obtained from Fig. 2 when the current density was 100 μA/cm^2. V_c for the propagation of pits and corrosion were determined by potentiostatic polarization tests.

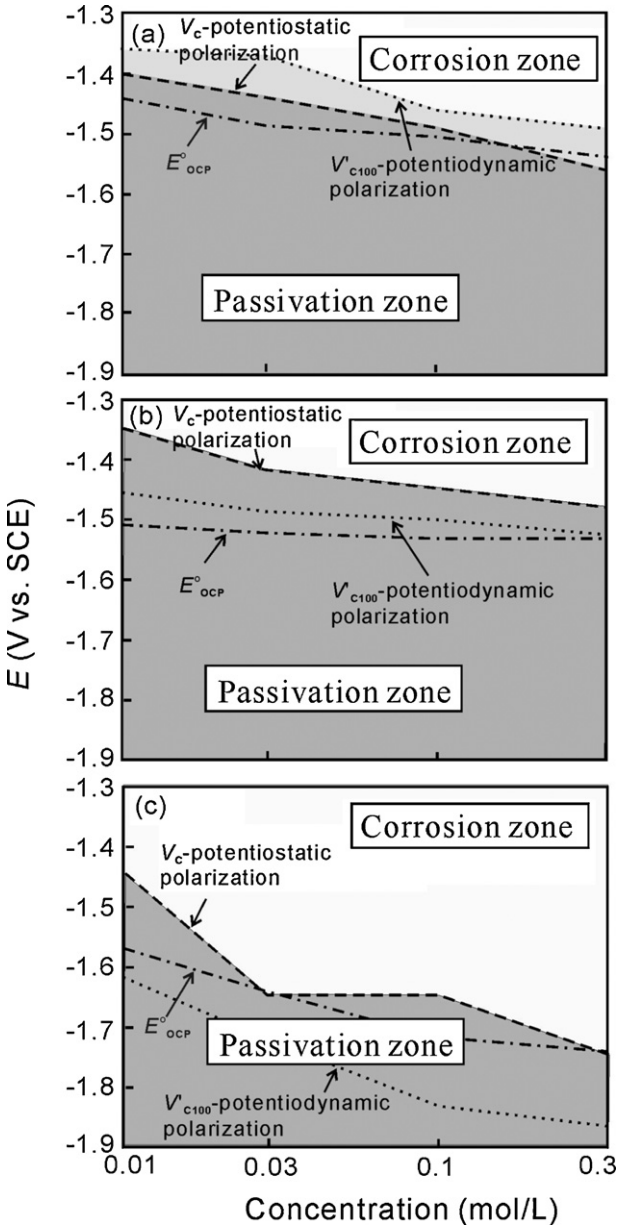

Fig. 6. Corrosion maps of AZ31 alloy in (a) NaCl [16], (b) Na_2SO_4 and (c) $NaHCO_3$ solutions, in which corrosion and passivation zones correspond to electrochemical measurements.

As viewed in Fig. 6, the V_c values in NaCl are slightly lower than the V'_{c100} ones due to the induction time. Conversely, V_c values in Na_2SO_4 and $NaHCO_3$ are higher than V'_{c100} values, which is consistent with the maximum in the early stage of potentiostatic polarization. V_c is the main boundary which divides corrosion and passivation zones. It is noted that once V_c is reached, the incorporated anions (Cl^-, SO_4^{2-}) rupture the passive film at these defect sites, reach the base metal surface and initiate pitting [29,30]. Propagation and growth of pitting corrosion result from changes in solution chemistry within pit cavity [31]. Concentration changes in solution inside pit cavity occur when magnesium cations enter solution bringing about an increase in anions (Cl^-, SO_4^{2-}) concentration by migration. The solution inside pits in this way becomes aggressive and allows active dissolution of AZ31 alloy via the formation of soluble corrosion products, possibly composed of $Mg(OH)_2$. These soluble corrosion products could be removed from pits by diffusion [17,18]. In addition, referring again to Fig. 3, such pro-

Table 2
Corrosion rates of AZ31 alloy polarized potentiostatically at −1.35 V after 72 ks in 0.01 mol/L NaCl, Na_2SO_4 and $NaHCO_3$ solutions.

Solution	Corrosion rate ($g\,m^{-2}\,h^{-1}$)	Corrosion current density ($\mu A\,cm^{-2}$)
NaCl	0.47	373.30
Na_2SO_4	0.32	251.04
$NaHCO_3$	0.12	92.05

moting effect of polarized potential above on the corrosion process can be explained that an increase in polarized potential accelerates the rates of migration and diffusion of the reactant and product species into and from pits.

The passivation zones become narrow with increasing [Cl^-], [SO_4^{2-}] and [HCO_3^-] for all the specimens. The specimen in Na_2SO_4 exhibits the broadest zone followed by NaCl and $NaHCO_3$. The E^0_{ocp} values shift to less noble potentials with increasing solution concentrations. This is attributed to the easier anodic dissolution of the surface film in more concentrated solutions. Meanwhile, the E^0_{ocp} values of AZ31 are in the passivation zone when [Cl^-] is less than 0.2 mol/L, and [SO_4^{2-}] and [HCO_3^-] are less than 0.3 mol/L, respectively. The surface films or the corrosion products covering the surface may play protective role and retard further corrosion in dilute solutions. In $NaHCO_3$, an anodic film $MgCO_3$ was found to cover the surface by X-ray diffraction with high peak intensity (not shown), which is thicker than the $Mg(OH)_2$ film. The $MgCO_3$ film may stop the hydrogen evolution process and interfere with both anodic and cathodic reactions.

Table 2 shows the corrosion rates of AZ31 polarized potentiostatically at −1.35 V (in corrosion state III) in 0.01 mol/L NaCl, Na_2SO_4 and $NaHCO_3$ solutions as calculated by Faraday's laws [32]. The corrosion current densities are obtained from potentiostatic polarization after 72 ks (Fig. 3). The corrosion rate in $NaHCO_3$ (general corrosion) is three times and four times less than the rates in Na_2SO_4 and NaCl (localized corrosion), which is confirmed the results as described in Fig. 5. This low corrosion rate indicates that a specific insoluble salt precipitation contributes to the surface layer formation on the material, which retards Mg^{2+} dissolution by inhibiting mass diffusion. Yamamoto and Hiromoto [24] reported that the total Mg^{2+} release in NaCl + $NaHCO_3$ was lower than that in NaCl + HEPES (N-2-hydroxyethylpiperazine-N′-2-ethane sulfonic acid). The precipitation of $MgCO_3$ is effective in improving the corrosion resistance of magnesium in a neutral solution with a carbonate–bicarbonate system.

Fig. 7 illustrates the log [Mg^{2+}]–pH diagrams constructed for Mg–H_2O and Mg–CO_2 systems. The Mg corrosion in a neutral solution proceeds as follows [33]:

$$Mg(s) \rightarrow Mg^{2+}(aq) + 2e^- \quad (1)$$

$$2H_2O + 2e^- \rightarrow H_2 + 2OH^- \quad (2)$$

In NaCl and Na_2SO_4, surface water will react with the film according to Eq. (3) since $MgCl_2$ and $MgSO_4$ are soluble.

$$Mg^{2+}(aq) + 2OH^-(aq) \rightarrow Mg(OH)_2(s) \log K_c = 11.07 \quad (3)$$

The thermodynamic equilibrium equation would be (Fig. 7(a))

$$\log[Mg^{2+}] = 16.93 - 2\ pH \quad (4)$$

It is proposed that a magnesium carbonate product is formed in $NaHCO_3$.

$$Mg^{2+}(aq) + HCO_3^-(aq) + OH^-(aq) \rightarrow MgCO_3 + H_2O \log K_c = 8.7 \quad (5)$$

The thermodynamic equilibrium equation would be

$$\log[Mg^{2+}] + \log[HCO_3^-] = 5.3 - pH \quad (6)$$

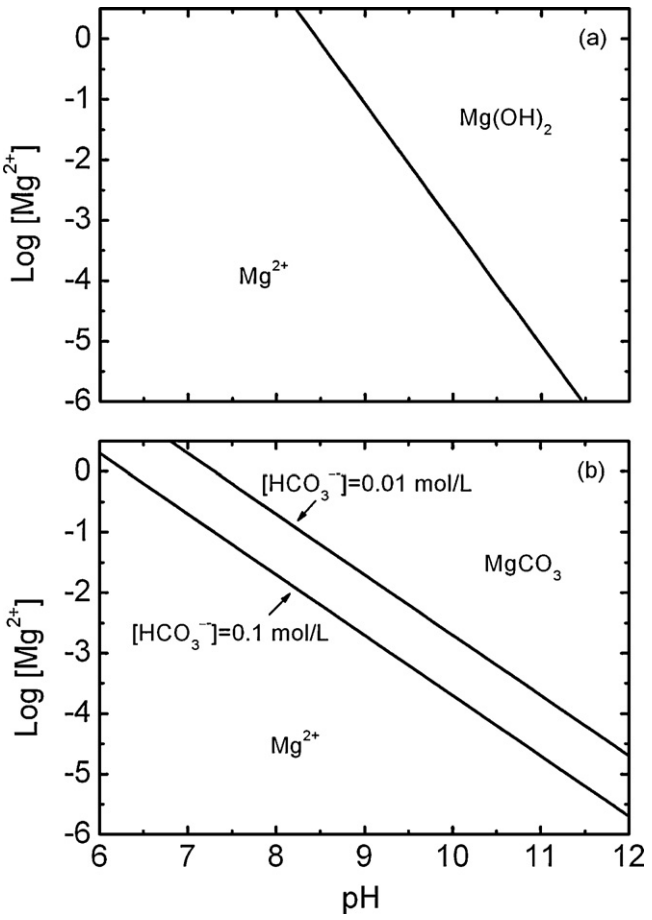

Fig. 7. Thermodynamic stability of $Mg(OH)_2$ formed in aqueous solution (a) and $MgCO_3$ formed in $NaHCO_3$ solution (b).

In the log [Mg^{2+}]–pH diagram, the stable zone of $MgCO_3$ becomes wider with increasing [HCO_3^-] (Fig. 7(b)). It should be noted that $MgCO_3$ is more stable with increasing [HCO_3^-] as compared to $Mg(OH)_2$ (Fig. 7(a)). Baril and Pébère [34] found that the CO_3^{2-} ion enhanced the de-stabilization of $Mg(OH)_2$/MgO layer when [CO_3^{2-}] was relatively low as 4.76×10^{-4} mol/L. It suggests that CO_3^{2-} ion was effective in retarding Mg dissolution by forming an insoluble $MgCO_3$ layer on the material when ion concentration was high enough [18], such as 0.01 mol/L. In addition, Song et al. [19] suggested that the stability of a surface film depended on the solution pH value, in which a higher pH value solution made the surface film more passive. In our study, we found that the E_{ocp} value in $NaHCO_3$ shows the lowest value as compared to NaCl and Na_2SO_4 (Fig. 1), which is attributed to the low pH of surface film in $NaHCO_3$.

4. Conclusions

(1) Corrosion maps were obtained for AZ31 alloy in dilute Na_2SO_4 and $NaHCO_3$ solutions on the basis of electrode potential and ion concentration determined by electrochemical measurements. These results were compared with the corrosion map in NaCl in previous work. The specimens exhibited corrosion and passivation zones. The passivation zone was strongly influenced by the kinds of the solution used.
(2) Based on the corrosion maps, the broadest passivation zone was obtained in Na_2SO_4, followed by NaCl and $NaHCO_3$. AZ31 alloy had a better corrosion resistance in Na_2SO_4, attributing to the lowest attack by SO_4^{2-} and the thick corrosion product formed on the surface which inhibited the corrosion attack.

However, the corrosion rate in $NaHCO_3$ was lower than the rates in NaCl and Na_2SO_4, even though the lowest passivation zone was exhibited by the former. The values of open-circuit potential were in the passivation zone when [Cl^-] was less than 0.2 mol/L in NaCl, and [SO_4^{2-}] and [HCO_3^-] were both less than 0.3 mol/L in Na_2SO_4 and $NaHCO_3$.

(3) In the passivation zone, the formation of the surface films or corrosion products on the material retarded further corrosion in dilute solutions. In the corrosion zone, pits grew continuously both in depth and diameter in NaCl and Na_2SO_4. This led to the localized corrosion through the agglomeration of pits. The formation of crystalline-like $MgCO_3$ products exhibited the general corrosion in $NaHCO_3$.

References

[1] O. Lunder, J.E. Lein, S.M. Hasjevik, T.Kr. Aune, K. Nisanciglu, Werkstoffe und Korrosion 45 (1994) 331–340.
[2] G. Song, A. Atrens, M. Dargusch, Corros. Sci. 41 (1998) 249–273.
[3] R. Ambat, N.N. Aung, W. Zhou, Corros. Sci. 42 (2000) 1433–1455.
[4] Z.M. Shi, G. Song, A. Atrens, Corros. Sci. 48 (2006) 1939–1959.
[5] T. Zhang, Y. Shao, G. Meng, F. Wang, Electrochim. Acta 53 (2007) 561–568.
[6] G. Ballerini, U. Bardi, R. Bignucolo, G. Ceraolo, Corros. Sci. 47 (2005) 2173–2184.
[7] G. Song, A. Atrens, X.L. Wu, B. Zhang, Corros. Sci. 40 (1998) 1769–1791.
[8] A. Pardo, M.C. Merino, A.E. Coy, R. Arrabal, F. Viejo, E. Matykina, Corros. Sci. 50 (2008) 823–834.
[9] S. Feliu Jr., A. Pardo, M.C. Merino, A.E. Coy, F. Viejo, R. Arrabal, Appl. Surf. Sci. 255 (2008) 4102–4108.
[10] T. Shinohara, L. Wang, Proc. JSCE Mater. Environ. (2008), p. C-310.
[11] M.C. Zhao, M. Liu, G.L. Song, A. Atrens, Corros. Sci. 50 (1998) 1939–1953.
[12] A. Pardo, M.C. Merino, A.E. Coy, F. Viejo, R. Arrabal, S. Feliu Jr., Electrochim. Acta 53 (2008) 7890–7902.
[13] J. Chen, J.H. Dong, J.Q. Wang, E.H. Han, W. Ke, Corros. Sci. 50 (2008) 3610–3614.
[14] N. Liu, J.L. Wang, L.D. Wang, Y.M. Wu, L.M. Wang, Corros. Sci. 51 (2009) 1328–1333.
[15] Y.W. Song, D.Y. Shan, R.S. Chen, E.H. Han, Corros. Sci. 51 (2009) 1087–1094.
[16] L. Wang, T. Shinohara, B.P. Zhang, Corros. Eng. Jpn. 58 (2009) 105–110.
[17] S. Hiromoto, A. Yamamoto, N. Maruyama, H. Somekawa, T. Mukai, Corros. Sci. 50 (2008) 3561–3568.
[18] S. Hiromoto, A. Yamamoto, N. Maruyama, H. Somekawa, T. Mukai, Mater. Trans. 49 (2008) 1456–1461.
[19] G. Song, A. Atrens, D. St John, X. Wu, J. Nairn, Corros. Sci. 39 (1997) 1981–2004.
[20] E. Brillas, P.L. Cabot, F. Centellas, J.A. Garrido, E. Perez, R.M. Rodriguez, Electrochim. Acta 43 (1998) 799–812.
[21] J.H. Dong, T. Nishimura, T. Kodama, Mater. Res. Soc. 713 (2002), JJ11.8.1.
[22] M.A. Amin, S.S. Abd El-Rehim, E.E.F. El-Sherbini, S.R. Mahmoud, M.N. Abbas, Electrochim. Acta 54 (2009) 4288–4296.
[23] S. Hiromoto, T. Shishido, A. Yamamoto, N. Maruyama, H. Somekawa, T. Mukai, Corros. Sci. 50 (2008) 2906–2913.
[24] A. Yamamoto, S. Hiromoto, Mater. Sci. Eng. C 29 (2009) 1559–1568.
[25] H. Bohni, H.H. Uhlig, J. Electrochem. Soc. 116 (1969) 906–910.
[26] L. Wang, T. Shinohara, B.P. Zhang, H. Iwai, J. Alloys Compd. 485 (2009) 747–752.
[27] R. Lindström, L.-G. Johansson, G.E. Thompson, P. Skeldon, J.-E. Svensson, Corros. Sci. 46 (2004) 1141–1158.
[28] M. Pourbaix, Werkstoffe und Korrosion 11 (1960) 761–766.
[29] S.-i. Pyun, S.-M. Moon, S.-H. Ahn, S.-S. Kim, Corros. Sci. 41 (1999) 653–667.
[30] M.A. Amin, S.S. Abd El-Rehim, E.E.F. El-Sherbini, S.R. Mahmoud, M.N. Abbas, Electrochim. Acta 54 (2009) 4288–4296.
[31] D.D. Macdonald, K.M. Ismail, E. Sikora, J. Electrochem. Soc. 145 (1998) 3141–3149.
[32] D.L. Piron, The Electrochemistry of Corrosion, NACE, Houston, 1991, p. 75.
[33] H.P. Godard, W.B. Lepson, M.R. Bothewell, R.L. Kane, The Corrosion of Light Metals, Wiley, New York, 1967, p. 260.
[34] G. Baril, N. Pébère, Corros. Sci. 43 (2001) 471–484.